npj | quantum materials

Article

Published in partnership with Nanjing University

https://doi.org/10.1038/s41535-024-00640-8

Test for BCS-BEC crossover in the cuprate superconductors

Qijin Chen [1,2,3] ✉, Zhiqiang Wang [4], Rufus Boyack[5] & K. Levin [4] ✉

In this paper we address the question of whether high-temperature superconductors have anything in common with BCS-BEC crossover theory. Towards this goal, we present a proposal and related predictions which provide a concrete test for the applicability of this theoretical framework. These predictions characterize the behavior of the Ginzburg-Landau coherence length, $\xi_0^{\rm coh}$, near the transition temperature T_c, and across the entire superconducting T_c dome in the phase diagram. That we are lacking a systematic characterization of $\xi_0^{\rm coh}$ in the entire class of cuprate superconductors is perhaps surprising, as it is one of the most fundamental properties of any superconductor. This paper is written to motivate further experiments and, thus, address this shortcoming. Here we show how measurements of $\xi_0^{\rm coh}$ contain direct indications for whether or not the cuprates are associated with BCS-BEC crossover and, if so, where within the crossover spectrum a particular superconductor lies.

The subject of high-temperature superconductivity in the cuprates is by now a mature field with a diverse array of candidate theories. This applies as well to theories of the mysterious pseudogap which has captured the attention of the community. It is notable that there is still no consensus about the nature of the machinery and the mechanism behind this phenomenon. This should be clear from the large number of review articles[1–4], which represent a range of different perspectives and viewpoints. It can be plausibly argued that, as the field is so mature, what is most needed now is for candidate cuprate theories to formulate testable, preferably falsifiable predictions.

This is the goal of the present paper for one particular theory, called 'BCS-BEC crossover theory'. Here we address the question of whether high-temperature superconductors have anything in common with BCS-BEC crossover theory. We understand this to be a highly controversial issue, but note that this subject has received recent attention in the literature[5,6]. For this purpose, we focus on the Ginzburg-Landau (GL) coherence length, $\xi_0^{\rm coh}$, appropriate to near or slightly above T_c. In this paper we provide direct predictions for its behavior as a function of hole doping. We argue that these predictions can be used to directly assess the appropriateness of BCS-BEC crossover theory for the cuprate family, when $\xi_0^{\rm coh}$ is measured systematically across the T_c dome in the phase diagram and for the different cuprate families.

This crossover theory has the advantage over many other cuprate theory candidates of potentially being applicable to a wide collection of strongly correlated superconductors. This broad range of applicability is exploited in the present work. Over the years we have acquired a knowledge base which has shown how to connect different types of experimental findings with 'crossover physics'. BCS-BEC crossover candidate materials include iron-based superconductors[7–14], organic superconductors[15–19], magic-angle twisted bilayer (MATBG)[20,21] and trilayer graphene (MATTG)[22,23], gate-controlled two-dimensional devices[24–26], interfacial superconductivity[27–29], and magneto excitonic condensates in graphene heterostructures[30].

The theory of BCS-BEC crossover[2,31–36] belongs to a class of preformed-pair theories associated with relatively strong 'pairing glue'. As a result, fermion pairs form at a higher temperature before they Bose condense at the superfluid transition temperature T_c, as found in the BEC phase of a Bose superfluid. Importantly, there is a continuous evolution between the two endpoints of a crossover theory: the conventional, weak-pairing BCS limit and the strong-pairing BEC limit. We emphasize that this theory pertains only to the machinery of superconductivity. It calls for a revision of the more familiar BCS approach, while still contemplating a charge $2e$ pairing-based scheme. It does not address the specific microscopic pairing mechanism.

Whether crossover theory is applicable to the cuprates or not is the question we wish to help address in the course of future experiments. That the transition temperature is high and there are indications that the GL coherence length (in comparison to traditional superconductors) is small

[1]Hefei National Research Center for Physical Sciences at the Microscale and School of Physical Sciences, University of Science and Technology of China, Hefei, Anhui 230026, China. [2]Shanghai Research Center for Quantum Science and CAS Center for Excellence in Quantum Information and Quantum Physics, University of Science and Technology of China, Shanghai 201315, China. [3]Hefei National Laboratory, University of Science and Technology of China, Hefei 230088, China. [4]Department of Physics and James Franck Institute, University of Chicago, Chicago, IL 60637, USA. [5]Department of Physics and Astronomy, Dartmouth College, Hanover, NH 03755, USA. ✉e-mail: qjc@ustc.edu.cn; levin@jfi.uchicago.edu

are argued[37] to be suggestive of strong pairing 'glue'. But it is clearly of interest to find more definitive and quantitative evidence for or against this scenario.

Here and in the vast literature on ultracold atomic Fermi gases[2,34,35], a superconductor/superfluid in the 'crossover' regime is conventionally viewed as belonging somewhere intermediate between BCS and BEC. There should be little doubt that the cuprates are not in the BEC limit. In this regime, all signs of fermionic physics have disappeared, which is clearly not the case for the cuprate superconductors; this point has been made recently by Sous et al.[6] in their analysis of the behavior of the fermionic chemical potential. The more relevant issue is whether the high-temperature superconductors can be described as belonging to an intermediate regime, somewhere between BCS and BEC and, if so, where in this spectrum a given cuprate might lie.

Indeed, even when a superconductor is on the fermionic side of the crossover, it can behave in a rather anomalous fashion both above and below T_c. We list here three necessary conditions for this crossover scenario to apply. (i) It is associated with the presence of a fermionic excitation gap or 'pseudogap' which has a temperature onset, T^*, substantially above T_c (say, $T^*/T_c \gtrsim 1.2$). (ii) It is also associated with sizable ratios of the zero-temperature gap to Fermi energy, Δ_0/E_F, (say, $\Delta_0/E_F \gtrsim 0.1$) and finally (iii) it has an anomalously small GL coherence length (say, $k_F\xi_0^{coh} \lesssim 30$, where k_F represents the ideal-gas measure of the carrier density).

In this context, it should be noted that large T^*/T_c is a necessary but not sufficient criterion for a pairing pseudogap, as there are alternative reasons why this ratio might be large[38]. On the other hand, a moderately large Δ_0/E_F may be more indicative of BCS-BEC crossover, but this ratio can be rather complicated to assess. This is because E_F is usually hard to quantify in a typical superconductor, as it is related to complex band structures. And for the cuprates one would presumably have to quantify this ratio over the entire T_c dome as a function of hole doping.

This leaves the GL coherence length as arguably the most useful parameter for characterizing BCS-BEC crossover. This length scale, which essentially reflects normal-state pairing correlations, should not be confused with other length scales such as the London penetration depth, which characterizes the superconducting components of the system. To be specific, the zero-temperature London penetration depth is related to the density-to-mass ratio of the constituent fermions, which is independent of pairing correlations (here, for simplicity, we consider a 3D superconductor in free space). We also emphasize here that in the crossover regime, this coherence length deviates from its BCS-limit expression and that it is similarly distinct from a measure of the size of the Cooper pairs.

Results

Coherence length in BCS-BEC crossover

A recent paper[19] on a candidate organic superconductor has provided a template of the coherence length for us to use here in presenting predictions for the cuprates. This is shown in Fig. 1a where the dimensionless coherence length $k_F\xi_0^{coh}$ is plotted across the entire T_c dome. Here the nominal Fermi momentum k_F simply reflects the carrier density. For this particular organic superconductor, pressure is used as a tuning parameter to effect the crossover between the weak-coupling and strong-pairing limit.

A central result of the present paper is establishing the counterpart behavior of Fig. 1a for the cuprates, particularly for the entire range of hole doping over the T_c dome. This is shown in Fig. 1b. Indeed, the GL coherence length has become a preferred quantity to measure for many of the newer BCS-BEC candidate systems[22,24].

The coherence length that we are interested in here can be obtained in several different ways. In principle, it enters into the slope of the upper critical magnetic field, H_{c2}, very near T_c:

$$\left.\frac{dH_{c2}}{dT}\right|_{T=T_c} = -\frac{\Phi_0}{2\pi T_c(\xi_0^{coh})^2} \quad \text{with} \quad \Phi_0 = \frac{hc}{|2e|}.$$

This is based on using the temperature-dependent coherence length $\xi_0^{coh}(T)$, which is defined in terms of the quantity of interest, ξ_0^{coh}, as $\xi_0^{coh}(T) = \xi_0^{coh}/\sqrt{(T_c - T)/T_c}$ as in conventional superconducting fluctuation theories. As discussed in the context of MATTG[22], extracting ξ_0^{coh} experimentally from dH_{c2}/dT is not entirely straightforward as it involves determining $T_c(H)$ in the presence of a substantial field-induced broadening of the transition.

Alternatively, in line with the philosophy in this paper, one can avoid some of these complications by determining the GL coherence length through studies of the fluctuation magnetotransport[39] in the normal state above T_c. Such experiments are generally performed in combination with theoretical analyses based on the Aslamazov-Larkin (AL) pairing fluctuations[40,41].

Theory overview

We next evaluate the GL coherence length within BCS-BEC crossover theory. In the presence of a vector potential, the effects from non-condensed pairs (and the associated pseudogap) are inhomogeneous, and thus directly evaluating $H_{c2}(T)$ to extract ξ_0^{coh} poses a great challenge to theory. By contrast, here we deduce the coherence length alternatively based on (normal-state) fluctuation theory[42,43]. Superconducting fluctuations are generally associated with AL contributions[40] which reflect bosonic or pairing degrees of freedom. Their contributions[40] to transport and thermodynamics generally scale as powers of $\epsilon \equiv (T - T_c)/T_c$ or the effective chemical potential of the pairs.

There is a rather direct association between the AL treatment of conventional weak-pairing fluctuations and that deriving from the strong-pairing regime. The conventional fluctuation propagator[40] depends on two

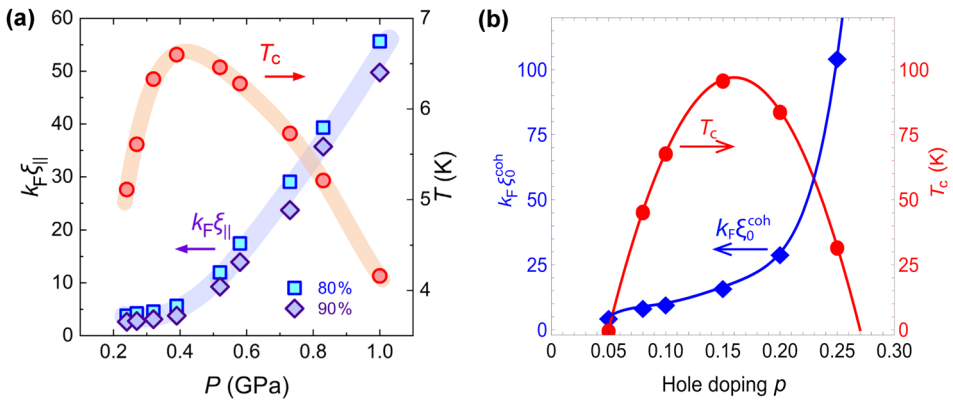

Fig. 1 | Comparison between experiment and theory for the in-plane coherence length and the T_c dome. a Pressure dependence of the measured in-plane coherence length $k_F\xi_0^{coh}$ near T_c, and superconducting transition temperatures in κ-(BEDT-TTF)$_4$Hg$_{2.89}$Br$_8$, taken from ref. 19. Here k_F is determined from the carrier density measured by the Hall coefficient. The T_c dome with overlain coherence length provides a rather ideal prototype for BCS-BEC crossover physics. **b** Calculated in-plane Ginzburg-Landau coherence length, based on fits to the cuprate phase diagram in Fig. 3. This coherence length should be associated with measurements at very low magnetic fields and near $T \approx T_c$. The red circles indicate the selected hole concentrations on the $T_c \sim p$ dome where both T^* and T_c were simultaneously fitted to yield the computed coherence lengths (blue diamonds).

parameters, ϵ and $\xi_0^{\rm coh}$. Similarly, for strong pairing the pair propagator, called the t-matrix, depends on an analogous pair of parameters, the pair chemical potential $\mu_{\rm pair}$ and the inverse pair mass $M_{\rm pair}^{-1}$. While conventional fluctuation transport calculations are complex[40], the central parameters ϵ and $\xi_0^{\rm coh}$ are essentially all that is needed to arrive at the entire collection of transport coefficients. Importantly, those calculations serve as a template for doing transport in the strong-pairing regime[44,45], provided one makes the association $\epsilon \to |\mu_{\rm pair}|/T_{\rm c}$ and similarly relates the pair mass $M_{\rm pair}$ to the coherence length $\xi_0^{\rm coh}$ within the strong-pairing theory via

$$\hbar^2 / \left[2M_{\rm pair}(T_{\rm c}) \left(\xi_0^{\rm coh} \right)^2 \right] = k_{\rm B} T_{\rm c}. \quad (1)$$

It should not be surprising then that (because BCS theory and its BCS-BEC crossover extension treat the Cooper pair degrees of freedom as quasi-ideal bosons interacting indirectly only via the constituent fermions), the expression for the transition temperature $T_{\rm c}$ essentially follows that of an ideal Bose gas (see Methods). For three dimensions (3D), this is given by

$$T_{\rm c} = \left(\frac{2\pi}{\mathcal{C}} \right) \left[\frac{\hbar^2}{k_{\rm B}} \frac{n_{\rm pair}^{2/3}(T_{\rm c})}{M_{\rm pair}(T_{\rm c})} \right], \quad (2)$$

where $\mathcal{C} = \left[\zeta(3/2) \right]^{2/3}$ with $\zeta(s)$ the Riemann zeta function. In this equation, $n_{\rm pair}$ and $M_{\rm pair}$ represent the respective number density and mass of the preformed Cooper pairs, which will condense at the transition. These parameters must be determined self consistently (see Methods).

It then follows from Eqs. (1) and (2) that $\xi_0^{\rm coh}$ assumes a very simple form; it depends only on the non-condensed or normal-state pair density $n_{\rm pair}$ presumed at the onset of the transition:

$$k_{\rm F} \xi_0^{\rm coh} = 1.2 (n/n_{\rm pair})^{1/3}, \quad (3)$$

where $k_{\rm F}^3$ reflects the total particle density n.

It should be noted that the above discussion can be extended to 2D as well, leading to a similar conclusion for the GL coherence length[36]:

$$k_{\rm F} \xi_0^{\rm coh} = 1.6 (n/n_{\rm pair})^{1/2}. \quad (4)$$

For the quasi-2D cuprates, both $M_{\rm pair}$ and $\xi_0^{\rm coh}$ in Eq. (1) are naturally anisotropic, but here we are interested in the in-plane coherence length so that, as in experiment, only the in-plane parameters will be used throughout.

We note that the above equations are easy to understand physically. The GL coherence length is a length representing the effective separation between preformed pairs. It relates to the density of pairs at $T_{\rm c}$ as distinct from the pair size. In BCS theory there are almost no pairs present at $T_{\rm c}$ and the length which represents their average separation is necessarily very long. As pairing becomes stronger more pairs form and their separation becomes shorter. On a lattice, in the BEC regime their separation is bounded from below by the characteristic lattice spacing and $\xi_0^{\rm coh}$ approaches an asymptote set by the inter-particle distance as the system varies from BCS to BEC.

More importantly, the rather natural expressions for $k_{\rm F}\xi_0^{\rm coh}$ in Eqs. (3) and (4) also reveal the location of a given system within the BCS-BEC crossover. Since the number of pairs at $T_{\rm c}$ varies from approximately 0 in the BCS limit to $n/2$ in the BEC case, the GL coherence length provides a quantitative measure of where a given superconductor is within the BCS-BEC spectrum.

Application to the cuprates

In application to the cuprates it is useful first to present a $T_{\rm c}$ versus attraction strength $|U|$ phase diagram for the case of d-wave pairing symmetry. This is deduced[2,36,46] based on Eq. (2) for $T_{\rm c}$ [see Methods]. Here, for the pseudogap onset temperature T^* we use a straightforward mean-field theory. The results are shown in Fig. 2. What is notable here is the fact that, in contrast to the s-wave pairing in BCS-BEC crossover[36], for the case of a d-wave superconducting order parameter, the BEC regime is not generally accessible except when the underlying conduction band has an extremely low filling. Although not relevant to the cuprates which are near half-filling, there may be other BCS-BEC crossover candidate systems which exhibit a d-wave BEC phase.

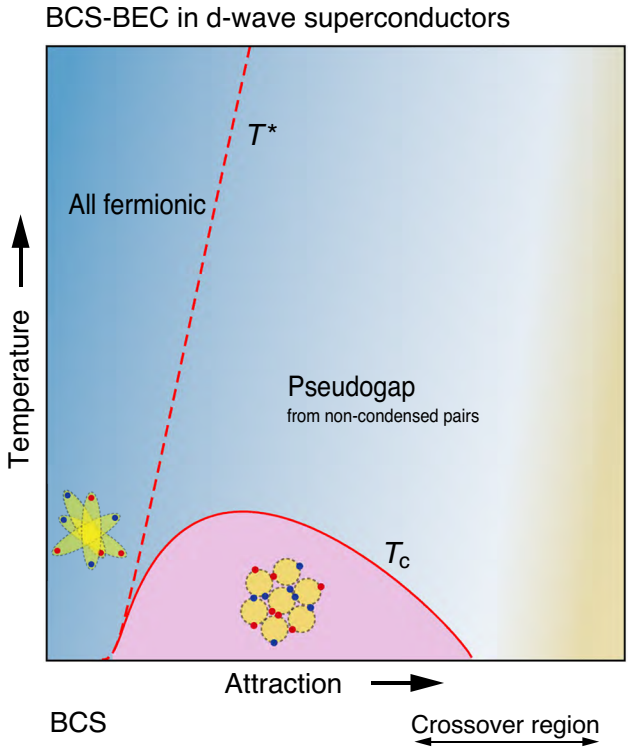

Fig. 2 | BCS-BEC crossover phase diagram for a d-wave superconductor with constant carrier density. This diagram[47] shows that the system (with a single electronic conduction band nearly half-filled) has vanishing $T_{\rm c}$ before the onset of the BEC regime, where the zero-temperature fermionic chemical potential drops below the band bottom. This can be compared with the low-density s-wave case in which the BEC regime is in principle accessible.

Heuristically, we understand the above contrast between $s-$ and $d-$ wave pairing as a consequence of the fact that d-wave pairs are more extended in size, so that multiple lattice sites are involved in the pairing. Consequently, repulsion between pairs is enhanced due to a stronger Pauli exclusion effect experienced by these extended pairs, and as a result their hopping is greatly impeded. Adding to this is the well known[33] observation that hopping of pairs on a lattice becomes more problematic in the strong-attraction regime, since the paired fermions have to unbind in the process. While in a low carrier density, s-wave pairing superconductor, $T_{\rm c}$ consequently approaches zero asymptotically in the BEC regime, generally for d-wave superconductors, $T_{\rm c}$ will vanish before the BEC limit is reached.

The above discussion brings us to the central topic of this paper: how one should determine whether the cuprates are associated with a BCS-BEC scenario and, if so, where a given cuprate precisely lies in the spectrum of BCS to BEC. Our proposal to quantitatively address this question is to focus on the calculated GL coherence length, with the goal of providing a counterpart plot like that in Fig. 1a, but now for the cuprates.

To that end, the first immediate task is to connect the d-wave crossover phase diagram in Fig. 2 with the experimental cuprate phase diagram in Fig. 3, where the horizontal axis is hole doping p, instead of $|U|$. To establish the connection, we fit the calculated T^* and $T_{\rm c}$ at a number of hole concentrations in the theory phase diagram to their corresponding experimental values, and deduce the associated properties of the GL coherence length. What is subtle but important here is that the phase diagram of Fig. 2 was

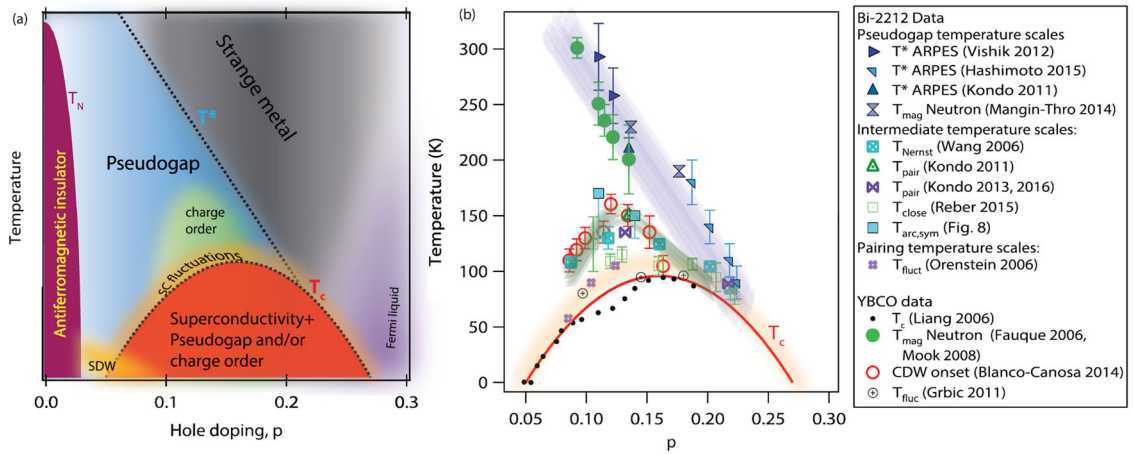

Fig. 3 | Experimental phase diagram for hole-doped cuprates, taken from ref. 57. T^* and T_c shown in (**a**) are quantitatively plotted in (**b**). The error bars in (**b**) represent the standard deviation.

obtained for a fixed carrier density. For application to the cuprates we need to readjust the density at each point in the $T_c \sim p$ dome.

To be specific, by taking the experimental T^*, T_c, and the corresponding density as input fitting parameters from Fig. 3, we can establish from T^*/T_c the magnitude of the attractive interaction ratio $|U|/t$, using the theoretical phase diagram in Fig. 2. Here t is the effective hopping parameter. Then fitting the numerical value of T^* yields the value of t, which determines the bandwidth and Fermi energy for each cuprate with a different hole concentration. From the fitted parameters $\{U, t\}$ and the hole concentration, we can compute (see Methods) $n_{\rm pair}$ and $M_{\rm pair}$, using our t-matrix theory[46,47], and then extract the coherence length.

For definiteness, we adopt a quasi-2D band structure considered to be appropriate for the cuprates: $\epsilon_{\mathbf{k}} = (4t + 4t' + 2t_z) - 2t(\cos k_x + \cos k_y) - 4t' \cos k_x \cos k_y - 2t_z \cos k_z$ with $t'/t = -0.3$. We presume a very small $t_z/t = 0.01$ is also present, but it should be stressed that T_c has only a very weak logarithmic dependence on t_z[47]. This band structure has a van Hove singularity which is prominent for the band fillings we address.

The predicted results for the GL coherence length based on our fitting procedure and BCS-BEC crossover theory are presented in Fig. 1b. These results show that, not unexpectedly, the coherence length is predicted to decrease monotonically with increased underdoping of holes, reflecting that the pairing strength is strongest in the most underdoped systems. Note that for the cuprates, the predicted minimum value of the coherence length is not particularly short. This more moderate value for $\xi_0^{\rm coh}$ in the underdoped regime is associated with the d-wave symmetry of the cuprates. In this doping regime, $n_{\rm pair}$, the number of pairs at the transition temperature T_c, remains far below its maximum possible value of $n/2$; stated alternatively, the corresponding $|U|/t$ at these hole concentrations is smaller than the value of $|U|/t$ where T_c vanishes (see Fig. 2). This implies that the underdoped cuprates are still well within the fermionic side of the crossover 'transition', which is defined as where $\mu = 0$ at T_c.

On the experimental side, in the earlier literature there is a prototypical set of experiments[39] which address $\xi_0^{\rm coh}$ in the immediate vicinity of the transition. Importantly, this analysis is based on a normal-state fluctuation analysis; as in a similar spirit to the theoretical calculation of $\xi_0^{\rm coh}$, this avoids difficulties associated with evaluating $dH_{c2}/dT|_{T=T_c}$ more directly. As seen in Fig. 14a of ref. 39, this analysis finds that in $La_{2-x}Sr_xCuO_4$ single-crystal films, there is a rather weak decrease of $\xi_0^{\rm coh}$ observed with increased underdoping. However, in the overdoped regime the measured coherence length is not as large as suggested in our Fig. 1b.

This and related research have emphasized that experiments based on standard fluctuation analyses below T_c are more problematic than above T_c. It is the shortness of the coherence length itself which is causing the difficulty. More specifically, the short coherence length results in a small characteristic energy associated with vortex pinning centers. This allows their motion to be more readily thermally activated. As a result, this enhanced vortex depinning significantly increases the width of the resistivity transition, making it difficult to determine the precise value of $T_c(H)$ and, similarly, $\xi_0^{\rm coh}$.

These $T \approx T_c$ studies which we focus on here should be contrasted with coherence-length measurements at low temperatures where use is made of the vortex core size[48,49]. Interestingly, here and in related transport experiments[50] there are similar challenges in measuring the coherence length which were attributed to the presence of a vortex liquid rather than vortex solid phase.

There are also other potential complications stemming from Fermi-surface reconstruction[51], which can be viewed as deriving from ordering in the particle-hole channel, seen at high magnetic fields H. If this reconstruction persists in the very low H limit, those regions of the T-p phase diagram where reconstruction appears will complicate the interpretation of $T_c(H)$ and, in turn, affect the inferred $\xi_0^{\rm coh}$. Indeed, it is now understood that three cuprate families ($YBa_2Cu_3O_{6+\delta}$, $La_{2-x}Sr_xCuO_4$, and $HgBa_2CuO_{4+\delta}$) each show significant Fermi-surface reconstruction in magnetic fields. These lead to non-monotonicity in the inferred[51–53] $H_{c2}(T = 0)$ and related $T = 0$ coherence length[49], as a function of hole doping. We note that for the $Bi_2Sr_2CaCu_2O_{8+\delta}$ family, by contrast, it appears from Nernst measurements that $H_{c2}(T)$ may not have these dramatic non-monotonicities in hole doping[54,55], from which one might presume that this family is not subject to Fermi surface reconstruction. Thus, these cuprates might be more suitable candidates for future experiments.

Fluctuation temperature scale in cuprates

There is another temperature scale besides T^* and T_c apparent in the phase diagram of Fig. 3 which, for completeness, needs to be addressed within the crossover scenario. We interpret this additional temperature scale in Fig. 3 as[36] the onset temperature for superconducting fluctuations which, as a function of hole doping in the cuprates, is observed to follow T_c, although remaining well separated.

It should be clear that within the crossover scheme the cuprates cannot be described by conventional fluctuation theory owing to the existence of a pairing gap onset temperature, T^*, significantly higher than T_c. That is, in the presence of a pseudogap associated with preformed pairs, the pairs are present over a much wider temperature range than in conventional fluctuation theory.

More specifically, as in fluctuation theories[40,41], fluctuation contributions in the crossover scenario derive from bosonic or pair degrees of freedom; they have an onset temperature which we define as $T_{\rm fluc} = T_c + \delta T_c$. This is expected to be significantly below the pseudogap onset T^*. At this latter temperature, a gap in the fermionic excitation spectrum first starts to appear, reflecting the onset of pair formation. That

$T_{\rm fluc}$ and T^* are distinct temperatures is a consequence of the fact that there must be an appreciable number of pairs before they are clearly observable in thermodynamical properties and transport.

For the case of conventional fluctuations, $T_{\rm fluc}$ can be associated with the characteristic size of the critical region, which can be related to G_i, the Ginzburg-Levanyuk number. This is, of course, extremely small in 3D although somewhat larger in 2D. (For conventional fluctuation theory[40], in 3D, $\delta T_c/T_{c0} \approx \sqrt{G_i}$, with $G_i \sim 80(T_c/E_F)^4$. In 2D, $\delta T_c/T_{c0} \approx G_i \ln 1/G_i$, with $G_i \approx T_c/E_F$. Here, T_{c0} is the mean-field transition temperature.)

In the crossover scenario one can address this somewhat different fluctuation picture in a more quantitative fashion. The onset temperature ($T_{\rm fluc}$) for pair-fluctuation effects on thermodynamics and transport requires sufficiently small but non-vanishing[56] values for the pair chemical potential, $|\mu_{\rm pair}|$. In this way, δT_c represents the temperature range over which non-condensed pairs are present in moderate quantity. Our discussion in this section has thus emphasized that the onset temperature for fluctuations is necessarily distinct, not only from T_c, but also from T^*.

Discussion

This paper is motivated by the observation that, because there are so many disparate approaches to understanding high-temperature cuprate superconductivity with as yet no consensus, for future progress it is important to subject candidate theories to falsifiability tests as much as is possible. Here we address one particular scenario: the BCS-BEC crossover picture. This has an added advantage among cuprate theories of being experimentally realized both in Fermi gas superfluids[2,34,35] and in a broader class of strongly correlated superconductors[36], which include some organic superconductors, twisted graphene families, interfacial superconductors and gated superconducting devices. These systems provide an instructive knowledge base for what to expect with different experimental probes. Importantly, with this knowledge base we have learned how to address the applicability of crossover theory[36].

In this paper, we have argued that the GL coherence length $\xi_0^{\rm coh}$ is a preferred parameter for assessing the appropriateness of BCS-BEC crossover theory for the cuprate family, when it is measured systematically across the T_c dome in the phase diagram and for the different cuprate families. We emphasize that this coherence length corresponds to temperatures around and slightly above T_c as it is associated with normal-state pairs. This is necessarily different from the size of Cooper pairs and also from the BCS expression for the zero-temperature coherence length: $\xi_0^{\rm BCS} = \hbar v_F/(\pi\Delta_0)$ where v_F is the Fermi velocity and $\Delta_0 = \Delta^{\rm BCS}(T=0)$. That the behavior is different from BCS theory should be obvious as BCS theory does not contain preformed pairs. Note also that the coherence length extracted at $T \gtrsim T_c$ in the cuprates should also not be confused with a counterpart measured in the ground state which has very different properties, relating to the superconducting condensate.

This same GL coherence length has been extensively studied in other BCS-BEC crossover candidate systems. Indeed, one can see by comparing the behavior for the organic superconductor in Fig. 1a with the prediction in Fig. 1b for the cuprates that these plots are rather similar, although the horizontal axes represent different variables. For the cuprates, one sees that the GL coherence length is predicted to monotonically decrease with increased underdoping, which reflects the fact that the pairing strength is strongest in the most underdoped systems. Also predicted in Fig. 1b is that the minimum value of the coherence length will not be as short as for the organic family, which seems to suggest these latter systems are closer to the BEC regime.

It is important to note that for assessing the appropriateness of a BEC scenario where fermions are absent, there are more direct experiments. Rather than focusing on the coherence length, one can study the chemical potential to determine whether, as would be expected, all signs of a Fermi surface have disappeared. Using this approach, recent work[6] has demonstrated that the cuprates are nowhere near the BEC endpoint of the crossover, where the chemical potential approaches the band bottom. Notably, however, the failure to observe BEC signatures does not constitute evidence for the 'the absence of BCS-BEC crossover'.

That in the cuprates we are lacking a systematic characterization of the GL coherence length $\xi_0^{\rm coh}$, over the entire class of cuprate superconductors, is perhaps surprising, as it is one of the most fundamental properties of any superconductor. Moreover, with very few exceptions, detailed measurements of $\xi_0^{\rm coh}$ have been used to provide support for or against a BCS-BEC crossover scenario in nearly all other candidate superconductors that have been studied[36]. This serves to emphasize how central a role $\xi_0^{\rm coh}$ has played, and the importance of further experiments on cuprates. In the process, these types of experiments will clarify the relevance (or lack thereof) of the BCS-BEC crossover scenario for the high-transition temperature copper-oxide superconductors.

Methods

Theory underlying BCS-BEC crossover

To determine the GL coherence length within BCS-BEC crossover theory, it is useful to summarize a few simple equations. We adopt the particular version of BCS-BEC crossover theory which builds on the $T = 0$ BCS ground state,

$$\Psi^{\rm BCS} = \Pi_{\mathbf{k}} \left(u_{\mathbf{k}} + v_{\mathbf{k}} a^\dagger_{\mathbf{k},\uparrow} a^\dagger_{-\mathbf{k},\downarrow} \right) |0\rangle. \tag{5}$$

This state, originally devised for weak-coupling, can be readily generalized[31] to incorporate stronger pairing glue through a self-consistent calculation of the parameters $u_{\mathbf{k}}$ and $v_{\mathbf{k}}$, which can be determined in conjunction with the fermionic chemical potential μ as the pairing interaction is varied.

The coherence length, which appears in Eq. (1), depends on the pair density $n_{\rm pair}$ and pair mass $M_{\rm pair}$. These two quantities are important for arriving at the plots in Fig. 1b and Fig. 2. They must be determined self consistently and we do so here using a particular theory[2,36], designed to be consistent with Eq. (5) and its finite-temperature extension, as established by Kadanoff and Martin[46]. Within this theory one can show that Eq. (2) is equivalent to a generalized Thouless condition, which dictates that the bosonic chemical potential of preformed pairs, $\mu_{\rm pair}$, which enters into their propagator (called the t-matrix) must vanish at $T = T_c$. This generalized Thouless condition will, in turn, lead to a BCS-like gap equation (for T at T_c),

$$1 = (-U) \sum_{\mathbf{k}} \frac{1 - 2f(E_{\mathbf{k}})}{2E_{\mathbf{k}}} \varphi^2_{\mathbf{k}} |_{T=T_c}, \tag{6}$$

where $f(x) = \left[\exp\left(x/(k_B T)\right) + 1\right]^{-1}$ is the Fermi-Dirac distribution function, $E_{\mathbf{k}} = \sqrt{\xi^2_{\mathbf{k}} + |\Delta(T_c)\varphi_{\mathbf{k}}|^2}$ with $\xi_{\mathbf{k}} = \epsilon_{\mathbf{k}} - \mu$, and $\varphi_{\mathbf{k}} = \cos k_x - \cos k_y$ is the d-wave pairing symmetry form factor. Here, $-U > 0$ represents the strength of the attractive interaction. Note that the central change from strict BCS theory (aside from a self-consistent readjustment of the fermionic chemical potential) is that T_c is determined in the presence of a nonzero excitation gap, $\Delta(T_c)$, reflecting the non-condensed pairs.

The process of establishing Eq. (6) provides values for $n_{\rm pair}$ and $M_{\rm pair}$ associated with our extended form of BCS theory having a ground state of the form Eq. (5). While Thouless has argued that a divergence of a sum of 'ladder' diagrams (within a pair propagator) is to be associated with the BCS transition temperature, Kadanoff and Martin established that this Thouless condition can be extended to characterize the full BCS temperature-dependent gap equation for all $T \leq T_c$, provided one adopts a particular form for the pair propagator or t-matrix

$$\frac{1}{t(i\Omega_m, \mathbf{q})} = T \sum_n \sum_{\mathbf{k}} G(i\omega_n, \mathbf{k}) G_0(i\Omega_m - i\omega_n, \mathbf{q} - \mathbf{k}) + \frac{1}{U}, \tag{7}$$

The bare and dressed fermionic Green's functions in the above equation are respectively $G_0(i\omega_n, \mathbf{k}) = \left(i\omega_n - \xi_{\mathbf{k}}\right)^{-1}$ and $G(i\omega_n, \mathbf{k}) \equiv$

$\left[G_0^{-1}(i\omega_n,\mathbf{k})-\Sigma(i\omega_n,\mathbf{k})\right]^{-1}$, with $\Sigma(i\omega_n,\mathbf{k})=-\Delta^2 G_0(-i\omega_n,-\mathbf{k})$. $\hbar\omega_n=(2n+1)\pi k_B T$ and $\hbar\Omega_m=2m\pi k_B T$ are fermionic and bosonic Matsubara frequencies (times $\hbar$), respectively.

Calculation of pair mass and number density

We are now in a position to compute the pair mass and number density from $t(i\Omega_m,\mathbf{q})$. After analytical continuation, $i\Omega_m\to\Omega+i0^+$, we expand the (inverse) t-matrix for small argument Ω and $\mathbf{q}$ to find

$$t(\Omega,\mathbf{q})\approx\frac{Z^{-1}}{\Omega-\Omega_{\mathbf{q}}+\mu_{\rm pair}},\tag{8}$$

where the pair mass can be calculated from the pair dispersion $\Omega_{\mathbf{q}}=\hbar^2\mathbf{q}^2/(2M_{\rm pair})$. In this equation Z is a constant independent of Ω and $\mathbf{q}$. $\{M_{\rm pair},\mu_{\rm pair},Z\}$ are all functions of the fermionic gap Δ and chemical potential μ, which are in turn functions of $|U|$ and temperature T for given total carrier density n. Finally, one can obtain the density of non-condensed pairs by treating them as stable and independent bosons, for which we have

$$n_{\rm pair}=\sum_{\mathbf{q}}b(\Omega_{\mathbf{q}}-\mu_{\rm pair})=Z\Delta^2.\tag{9}$$

Here, $b(x)=\left[\exp\left(x/(k_BT)\right)-1\right]^{-1}$ is the Bose-Einstein distribution function. To derive the last equality in Eq. (9), we have used $\Delta^2=-T\sum_m\sum_{\mathbf{q}}t(i\Omega_m,\mathbf{q})$. Equation (9) is valid for $T\geq T_c$, while for $T<T_c$, where $\mu_{\rm pair}\equiv 0$, the $\mathbf{q}=0$ component, which represents condensed pairs, needs to be treated separately.

Right at $T=T_c$ and for given $\{|U|,n\}$, we solve the gap equation Eq. (6) and Eq. (9) with $\mu_{\rm pair}=0$, together with the total electron density constraint

$$n=\sum_{\mathbf{k}}\left[1-\frac{\xi_{\mathbf{k}}}{E_{\mathbf{k}}}\tanh\left(\frac{E_{\mathbf{k}}}{2k_BT}\right)\right],\tag{10}$$

to determine $\{T_c,\Delta(T_c),\mu(T_c)\}$. In this way we can map out the $T_c-|U|$ phase diagram for a given density n. The result is schematically shown in Fig. 2, where the pseudogap onset temperature T^* is obtained by solving the mean-field BCS T_c equation in the absence of non-condensed pairs. Furthermore, from the calculated μ and Δ we can compute $\{M_{\rm pair},\mu_{\rm pair}\}$ using Eq. (8). Then substituting the results into Eq. (1) gives us $\xi_0^{\rm coh}$ as a function of $|U|$ and n. In application to cuprate superconductors, we use the calculated T^*/T_c ratio to determine $|U|$ for given hole doping $p=1-n$, by following the fitting procedure outlined in the Section 'Application to the cuprates'. This allows us to determine $\xi_0^{\rm coh}$ as a function of hole doping p for the entire T_c dome as shown in Fig. 1b.

Data availability

The data analyzed in the current study are available from the author Qijin Chen on reasonable request.

Code availability

The codes used for the current study are available from the author Qijin Chen on reasonable request.

Received: 2 August 2023; Accepted: 4 March 2024;
Published online: 15 March 2024

References

1. Lee, P. A., Nagaosa, N. & Wen, X.-G. Doping a mott insulator: Physics of high-temperature superconductivity. *Rev. Mod. Phys.* **78**, 17 (2006).
2. Chen, Q. J., Stajic, J., Tan, S. N. & Levin, K. BCS? BEC crossover: From high temperature superconductors to ultracold superfluids. *Phys. Rep.* **412**, 1–88 (2005).
3. Keimer, B., Kivelson, S. A., Norman, M. R., Uchida, S. & Zaanen, J. From quantum matter to high-temperature superconductivity in copper oxides. *Nature* **518**, 179–186 (2015).
4. Fradkin, E., Kivelson, S. A. & Tranquada, J. M. Colloquium: Theory of intertwined orders in high temperature superconductors. *Rev. Mod. Phys.* **87**, 457 (2015).
5. Harrison, N. & Chan, M. K. Magic gap ratio for optimally robust fermionic condensation and its implications for high -T_c superconductivity. *Phys. Rev. Lett.* **129**, 017001 (2022).
6. Sous, J., He, Y. & Kivelson, S. A. Absence of a BCS-BEC crossover in the cuprate superconductors. *npj Quant. Mater.* **8**, 25 (2023).
7. Kasahara, S. et al. Giant superconducting fluctuations in the compensated semimetal FeSe at the BCS–BEC crossover. *Nat. Commun.* **7**, 12843 (2016).
8. Kasahara, S. et al. Field-induced superconducting phase of FeSe in the BCS-BEC cross-over. *Proc. Nat'l Acad. Sci. U.S.A.* **111**, 16309–16313 (2014).
9. Okazaki, K. et al. Superconductivity in an electron band just above the Fermi level: possible route to BCS-BEC superconductivity. *Sci. Rep.* **4**, 4109 (2014).
10. Mizukami, Y. et al. Thermodynamics of transition to BCS-BEC crossover superconductivity in $FeSe_{1-x}S_x$. *Commun. Phys.* **6**, 183 (2023).
11. Hanaguri, T. et al. Quantum vortex core and missing pseudogap in the multiband BCS-BEC crossover superconductor FeSe. *Phys. Rev. Lett.* **122**, 077001 (2019).
12. Shibauchi, T., Hanaguri, T. & Matsuda, Y. Exotic superconducting states in FeSe-based materials. *J. Phys. Soc. Jpn.* **89**, 102002 (2020).
13. Kang, B. L. et al. Preformed Cooper Pairs in Layered FeSe-Based Superconductors. *Phys. Rev. Lett.* **125**, 097003 (2020).
14. Faeth, B. D. et al. Incoherent Cooper pairing and pseudogap behavior in single-layer FeSe/$SrTiO_3$. *Phys. Rev. X* **11**, 021054 (2021).
15. McKenzie, R. H. Similarities between organic and cuprate superconductors. *Science* **278**, 820–821 (1997).
16. Imajo, S. et al. Extraordinary π-electron superconductivity emerging from a quantum spin liquid. *Phys. Rev. Res.* **3**, 033026 (2021).
17. Matsumura, Y., Yamashita, S., Akutsu, H. & Nakazawa, Y. Thermodynamic measurements of doped dimer-Mott organic superconductor under pressure. *Low. Temp. Phys.* **48**, 51–56 (2022).
18. Oike, H. et al. Anomalous metallic behaviour in the doped spin liquid candidate κ-$(ET)_4Hg_{2.89}Br_8$. *Nat. Commun.* **8**, 756 (2017).
19. Suzuki, Y. et al. Mott-driven BEC-BCS crossover in a doped spin liquid candidate κ-$(BEDT\text{-}TTF)_4Hg_{2.89}Br_8$. *Phys. Rev. X* **12**, 011016 (2022).
20. Cao, Y. et al. Unconventional superconductivity in magic-angle graphene superlattices. *Nature* **556**, 43–50 (2018).
21. Oh, M. et al. Evidence for unconventional superconductivity in twisted bilayer graphene. *Nature* **600**, 240–245 (2021).
22. Park, J. M., Cao, Y., Watanabe, K., Taniguchi, T. & Jarillo-Herrero, P. Tunable strongly coupled superconductivity in magic-angle twisted trilayer graphene. *Nature* **590**, 249–255 (2021).
23. Kim, H. et al. Evidence for unconventional superconductivity in twisted trilayer graphene. *Nature* **606**, 494–500 (2022).
24. Nakagawa, Y. et al. Gate-controlled BCS-BEC crossover in a two-dimensional superconductor. *Science* **372**, 190–195 (2021).
25. Saito, Y., Nojima, T. & Iwasa, Y. Highly crystalline 2D superconductors. *Nat. Rev. Mater.* **2**, 16094 (2016).
26. Nakagawa, Y. et al. Gate-controlled low carrier density superconductors: Toward the two-dimensional BCS-BEC crossover. *Phys. Rev. B* **98**, 064512 (2018).
27. Richter, C. et al. Interface superconductor with gap behaviour like a high-temperature superconductor. *Nature* **502**, 528–531 (2013).
28. Božović, I. & Levy, J. Pre-formed cooper pairs in copper oxides and $LaAlO_3/SrTiO_3$ heterostructures. *Nat. Phys.* **16**, 712–717 (2020).
29. Cheng, G. et al. Electron pairing without superconductivity. *Nature* **521**, 196–199 (2015).

30. Liu, X. et al. Crossover between strongly coupled and weakly coupled exciton superfluids. *Science* **375**, 205–209 (2022).
31. Leggett, A. J. Diatomic molecules and Cooper pairs. In Pekalski, A. & Przystawa, J. A. (eds.) *Modern Trends in the Theory of Condensed Matter*, vol. 115 of *Lecture Notes in Physics*, 13–27 (Springer-Verlag, Berlin, West Germany, 1980). Proceedings of the XVI Karpacz Winter School of Theoretical Physics, February 19 - March 3, 1979, Karpacz, Poland.
32. Eagles, D. M. Possible pairing without superconductivity at low carrier concentrations in bulk and thin-film superconducting semiconductors. *Phys. Rev.* **186**, 456–463 (1969).
33. Nozières, P. & Schmitt-Rink, S. Bose condensation in an attractive fermion gas: from weak to strong coupling superconductivity. *J. Low. Temp. Phys.* **59**, 195–211 (1985).
34. Giorgini, S., Pitaevskii, L. P. & Stringari, S. Theory of ultracold atomic Fermi gases. *Rev. Mod. Phys.* **80**, 1215–1274 (2008).
35. Randeria, M. & Taylor, E. Crossover from Bardeen-Cooper-Schrieffer to Bose-Einstein condensation and the unitary Fermi gas. *Annu. Rev. Condens. Matter Phys.* **5**, 209–232 (2014).
36. Chen, Q. J., Wang, Z. Q., Boyack, R., Yang, S. L. & Levin, K. When superconductivity crosses over: From BCS to BEC. arXiv:2208.01774 (2022).
37. Leggett, A. J. What do we know about high Tc? *Nat. Phys.* **2**, 134–136 (2006).
38. Chand, M. et al. Phase diagram of the strongly disordered *s*-wave superconductor NbN close to the metal-insulator transition. *Phys. Rev. B* **85**, 014508 (2012).
39. Suzuki, M. & Hikita, M. Resistive transition, magnetoresistance, and anisotropy in $La_{2-x}Sr_xCuO_4$ single-crystal thin films. *Phys. Rev. B* **44**, 249–261 (1991).
40. Larkin, A. I. & Varlamov, A. A.*Theory of Fluctuations in Superconductors*. International Series of Monographs on Physics (OUP Oxford, 2009).
41. Varlamov, A. A., Galda, A. & Glatz, A. Fluctuation spectroscopy: From rayleigh-jeans waves to abrikosov vortex clusters. *Rev. Mod. Phys.* **90**, 015009 (2018).
42. Patton, B. R. Fluctuation theory of the superconducting transition in restricted dimensionality. *Phys. Rev. Lett.* **27**, 1273–1276 (1971).
43. Ullah, S. & Dorsey, A. T. Effect of fluctuations on the transport properties of type-ii superconductors in a magnetic field. *Phys. Rev. B* **44**, 262 (1991).
44. Boyack, R., Chen, Q. J., Varlamov, A. A. & Levin, K. Cuprate diamagnetism in the presence of a pseudogap: Beyond the standard fluctuation formalism. *Phys. Rev. B* **97**, 064503 (2018).
45. Boyack, R., Wang, X. Y., Chen, Q. J. & Levin, K. Combined effects of pairing fluctuations and a pseudogap in the cuprate Hall coefficient. *Phys. Rev. B* **99**, 134504 (2019).
46. Kadanoff, L. P. & Martin, P. C. Theory of many-particle systems. II. Superconductivity. *Phys. Rev.* **124**, 670–697 (1961).
47. Chen, Q. J., Kosztin, I., Jankó, B. & Levin, K. Superconducting transitions from the pseudogap state: *d*-wave symmetry, lattice, and low-dimensional effects. *Phys. Rev. B* **59**, 7083–7093 (1999).
48. Wen, H. H. et al. Hole doping dependence of the coherence length in $La_{2-x}Sr_xCuO_4$ thin films. *Europhys. Lett.* **64**, 790 (2003).
49. Sonier, J. E. et al. Hole-doping dependence of the magnetic penetration depth and vortex core size in $YBa_2Cu_3O_y$: Evidence for stripe correlations near $\frac{1}{8}$ hole doping. *Phys. Rev. B* **76**, 134518 (2007).
50. Ando, Y. & Segawa, K. Magnetotransport properties of untwinned $YBa_2Cu_3O_y$ single crystals: novel 60-K-phase anomalies in the charge transport. *J. Phys. Chem. Solids* **63**, 2253–2257 (2002).
51. Chan, M. K. et al. Extent of fermi-surface reconstruction in the high-temperature superconductor $HgBa_2CuO_{4+\delta}$. *Proc. Natl Acad. Sci. U.S A.* **117**, 9782–9786 (2020).
52. Badoux, S. et al. Critical doping for the onset of Fermi-surface reconstruction by charge-density-wave order in the cuprate superconductor $La_{2-x}Sr_xCuO_4$. *Phys. Rev. X* **6**, 021004 (2016).
53. Wang, Y., Li, L. & Ong, N. P. Nernst effect in high-T_c superconductors. *Phys. Rev. B* **73**, 024510 (2006).
54. Wang, Y. et al. Dependence of upper critical field and pairing strength on doping in cuprates. *Science* **299**, 86–89 (2003).
55. Chang, J. et al. Decrease of upper critical field with underdoping in cuprate superconductors. *Nat. Phys.* **8**, 751–756 (2012).
56. Boyack, R., Wang, Z. Q., Chen, Q. J. & Levin, K. Unified approach to electrical and thermal transport in high-T_c superconductors. *Phys. Rev. B* **104**, 064508 (2021).
57. Vishik, I. M. Photoemission perspective on pseudogap, superconducting fluctuations, and charge order in cuprates: a review of recent progress. *Rep. Prog. Phys.* **81**, 062501 (2018).

Acknowledgements

We thank Steve Kivelson, John Sous, and Yu He for stimulating discussions. We also thank Yayu Wang for discussions on related experiments. This work was partially (K.L., Z.W.) supported by the Department of Energy (DE-SC0019216). Q.C. was supported by the Innovation Program for Quantum Science and Technology (Grant No. 2021ZD0301904). R.B. was supported by the Department of Physics and Astronomy, Dartmouth College.

Author contributions

K.L. conceived and supervised the project. Q.C. performed the computations. Q.C. and Z.W. contributed to the acquisition of the data and preparation of figures. All authors have contributed to the interpretation of the data and the drafting as well as the revision of the manuscript.

Competing interests

The authors declare no competing interests.

Additional information

Correspondence and requests for materials should be addressed to Qijin Chen or K. Levin.